JOURNAL OF Materials CHEMISTRY

New pyrochlore phases in the ternary oxide Tl–Sb–O

Young-Sik Hong*† and Keon Kim

Division of Chemistry and Molecular Engineering, Department of Chemistry, Korea University, Seoul 136-701, Korea. E-mail: youngsikh@yahoo.com

Received 23rd October 2000, Accepted 13th February 2001
First published as an Advance Article on the web 4th April 2001

A new series of pyrochlore phases in the ternary oxide Tl–Sb–O have been prepared at 650 °C in air and characterised by XRD, FT-IR, EDX, XPS, and density measurements. The unit cell parameters were continuously decreased from 10.3073(1) Å for Tl/Sb = 1/4 to 10.28204(8) Å for Tl/Sb = 1/2 as the content of Tl^{3+} cations was increased. The Rietveld analysis shows that Tl^{+}, Tl^{3+}, Sb^{3+}, and Sb^{5+} cations were positioned in the 32e, 16d, 96g, and 16c sites, respectively. The Tl^{3+} cations progressively incorporated into the 16d sites in the space group *Fd3m*, substituting for Sb^{3+} cations in the 96g sites. The FT-IR absorption band at around 570 cm^{-1}, corresponding to the Sb^{3+}–O′ stretching vibrational mode, confirmed the existence of Sb^{3+} cations in the asymmetric 96g sites. These Tl–Sb–O phases are formulated with the composition $(Tl^{+}_{2/3-2\delta})[Sb^{3+}_{1-y}Tl^{3+}_{y}]_{2/3}Sb^{5+}_{2}O_{6.33-\delta}$ ($\delta \sim 0.05$) and exhibit quite unique structural features with three types of A/A′ cations in the 16d, 32e, and 96g sites.

Introduction

Materials with the pyrochlore structure exhibit rich crystal chemistry and interesting physical properties such as fast ionic conductivity and giant magnetoresistance, which make some of them suitable candidates for application in fuel cells and magnetic materials.[1–4] The pyrochlore structure with the composition $A_2B_2O_6O'$ (or $A_2B_2O_7$) is described as follows: A in 16d, B in 16c, O in 48f and O′ in 8b sites in the space group *Fd3m*. This structure can be viewed as two interpenetrating networks, A_2O' and B_2O_6, as shown in Fig. 1(a). A large number of compounds with the composition $A'B_2O_6$ were also found to have the pyrochlore structure, where the A′ cations are normally located in 8b or 32e sites, Fig. 1(b).[5] In this respect, one can expect that the pyrochlore phases lie within the composition ranges of $A_2B_2O_6O'$–$A'B_2O_6$, depending on the polarizabilities, ionic radii, and ionic charges of the A, A′, and B cations.[6]

Compounds with post-transition metal cations such as Tl, Pb, and Bi have attracted much interest because of their different electrical properties due to their mixed valence states. Among them, many Tl-containing ternary oxides, Tl–M–O (M = Nb, Ta, Ru, Mn), have been reported. For example, the simultaneous presence of Tl^{+} and Tl^{3+} cations was confirmed in $Tl_2Nb_2O_{6+x}$ ($0 \leqslant x \leqslant 1$).[7,8] It is well known that the Tl^{+} and Tl^{3+} cations are located in 32e and 16d sites, as evidenced by $TlNbTeO_6$ and $Tl_2Mn_2O_6O'$.[4,5] Recently, the Sb-containing ternary oxides, Ag–Sb–O and Na–Sb–O,[9,10] have been also investigated, but only three compounds for the Tl–Sb–O phase, $Tl_{10}Sb_2O_{10}$, $TlSbO_3$, and $Tl_{0.51}Sb_{0.71}Sb_2O_6O'_{0.32}$, were characterised.[11] In particular, the oxidation states of the Sb cations in the pyrochlore phases, such as $K_{0.51}Sb_{0.67}Sb_2O_{6.26}$, $Cs_{0.31}(Sb_{0.57}Na_{0.31}Pb_{0.02}Bi_{0.01})(Ta_{1.88}Nb_{0.12})(O_{5.69}[OH,F]_{0.31})$-$(OH,F)_{0.69}$, and $(Ca,Mn,Na)_{1.12}Sb_{0.65}(Sb,Ti,Fe,Al)_2O_6(OH)_{0.91}$, were found to be +3 in 96g sites and +5 in 16c sites.[12–15] From the structural point of view, therefore, the oxidation states and crystallographic sites in Tl–Sb–O pyrochlore phases are proposed to be Tl^{+} in 8b or 32e, Tl^{3+} in 16d, Sb^{3+} in 96g, and Sb^{5+} in 16c sites. This is the reason why Tl–Sb–O phases are much more complex than other pyrochlores and they have not been extensively studied, even though they could exhibit lone-pair effects and/or charge ordering phenomena.

In this work, we have prepared new pyrochlore phases of the ternary oxides Tl–Sb–O and characterized their crystal structures. By considering the pyrochlore structures and compositions, we propose the new formula $(Tl^{+}_{2/3-2\delta})$-$[Sb^{3+}_{1-y}Tl^{3+}_{y}]_{2/3}Sb_2O_6O'_{1/3-\delta}$ with Tl/Sb = 1/4–1/2, where the cations written in round and square brackets are monovalent cations in the 32e and trivalent cations in 96g/16d sites, respectively, and the oxidation state of the Sb atoms in 16c sites is +5.

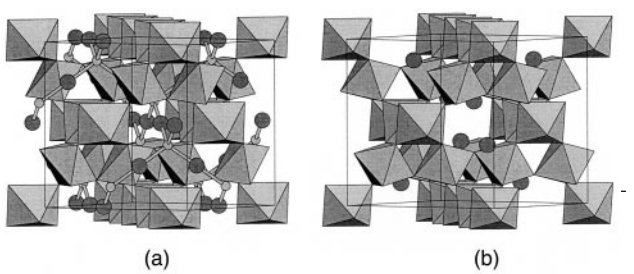

Fig. 1 Pyrochlore structures. (a) $A_2B_2O_6O'$ and (b) $A'B_2O_6$.

Experimental

The Tl–Sb–O phases were prepared by mixing Tl_2O_3 and Sb_2O_3 (Aldrich Chemicals, 99%) with Tl/Sb = 1/4, 1/3, and 1/2. After manual grinding, the mixture was poured into a platinum crucible and heated under air in a muffle furnace. The samples were first preheated at 450 °C for 12 h to prevent the evaporation of toxic thallium oxide and then, according to the TG analysis, these were thermally stable up to 750 °C. Finally the samples were heated at 600 °C for 12 h and then at 650 °C for 48 h. After each thermal treatment the products were quenched in air, weighed, ground, and examined by powder XRD method.

Powder XRD patterns were recorded at room temperature on a Philips X'pert APD using the Bragg–Brentano geometry with CuK_α radiation. Step scans were performed over the angular range $10 < 2\theta < 110°$ with a step size of 0.02° and a counting time of 10 s. Rietveld refinement was carried out with the help of the Fullprof program.[16] For each diffraction pattern, the scale factor, the counter zero point, the peak

asymmetry, and the unit cell parameter were refined in addition to the atomic parameters. The FT-IR spectra were recorded using a Bomen MB-102 spectrophotometer with the KBr-disc technique. Compositional analysis was conducted by using a JEOL JSM-5310LV SEM equipped with an EDX at an accelerating voltage of 20 keV. XPS were recorded on a Kratos XSAM 800 spectrometer by using MgK_{α} (1253.6 eV) radiation at 15 kV and 10 mA. Density measurements were carried out by a pycnometric method using bromobenzene as the immersion liquid.

Results

First of all, chemical characterisation should be accompanied by structural analysis such as the Rietveld method to clearly identify the Tl–Sb–O compounds, but the powders synthesized were not soluble in various acids and bases. For these compounds, the EDX and XPS analyses gave similar values to the nominal compositions as listed in Table 1. Although a little surface enrichment of antimony was observed at the powder surface, the nominal Tl/Sb ratio was used in the structural refinements because the compositional differences from EDX and XPS were not significant.

The powder XRD patterns of Tl–Sb–O phases are presented in Fig. 2. All the XRD reflections could be clearly indexed in the cubic system *Fd*3*m* with $Z=8$. It is worthwhile to note that the relative intensities of (311)/(222) decrease as the Tl/Sb ratio is increased, while the XRD patterns for the three compounds show similar features. This change seems to correlate with the relative occupation factor of Tl^{3+} and Sb^{3+} cations in the single crystal $Tl_{0.51}Sb_{2.71}O_{6.32}$, $\sim(Tl^{+}{}_{0.51})[Sb^{3+}{}_{0.71}]Sb_2O_6O'_{0.32}$, where the Sb^{3+} occupies the asymmetric 96g sites (x,x,z) near 16d (1/2,1/2,1/2).[7] In other words, the asymmetric Sb^{3+} cations are continuously substituted by the symmetric Tl^{3+} cations, accompanied by a change of the relative intensity of the (311)/(222) reflections in the XRD pattern.

To confirm this, the FT-IR spectra of Tl–Sb–O phases are shown in Fig. 3. The vibrational spectra may be of great use in characterising the change of local symmetry due to the substitution of Sb^{3+} cations by Tl^{3+}, because XRD patterns give a long-range order rather than short-range order. All the FT-IR spectra on the whole are analogous and five absorption bands are observed at $\sim$770, $\sim$700, $\sim$570, $\sim$430, and $\sim$360 cm^{-1}, respectively. According to the group analysis of the pyrochlore structure with the space group *Fd*3*m*, it is well known that there exist seven IR-active bands at about 700–600 cm^{-1} (B–O stretching), 500 cm^{-1} (A–O′ stretching), 400 cm^{-1} (A–O stretching), 300 cm^{-1} (O–B–O bending), 200 cm^{-1} (A–BO_6 stretching), 150 cm^{-1} (O–A–O bending) and 100 cm^{-1} (O′–A–O′ bending).[17] Then, the IR band at 570 cm^{-1} could be assigned as Sb^{3+}–O′ stretching mode, of which the absorption decreased from Sb_6O_{13} ($=Sb^{3+}Sb^{5+}{}_2O_{6.5}$) to the Tl/Sb = 1/2 phase, Fig. 3.

The observed, calculated, and difference XRD profiles of the Tl/Sb = 1/4 phase are shown in Fig. 4. The initial structural model was taken from the crystallographic data of single crystal $Tl_{0.51}Sb_{2.71}O_{6.32}$. Considering the constraints of composition and charge neutrality, the Tl^{+}, Sb^{3+}, Sb^{5+}, O, and O′ could be positioned in 32e, 96g, 16c, 48f, and 8b sites, giving the composition $(Tl^{+}{}_{0.67})[Sb^{3+}{}_{0.67}]Sb_2O_6O'_{0.34}$. However, the resulting agreement factors of $R_p=15.0\%$, $R_{wp}=15.5\%$, and $R_I=7.13\%$ were rather high. To improve the fit, some of the

Table 1 Chemical analysis of Tl–Sb–O phases

Tl/Sb	1/4	1/3	1/2
EDX	1 : 3.92	1 : 3.01	1 : 1.97
XPS	1 : 4.13	1 : 3.04	1 : 2.09

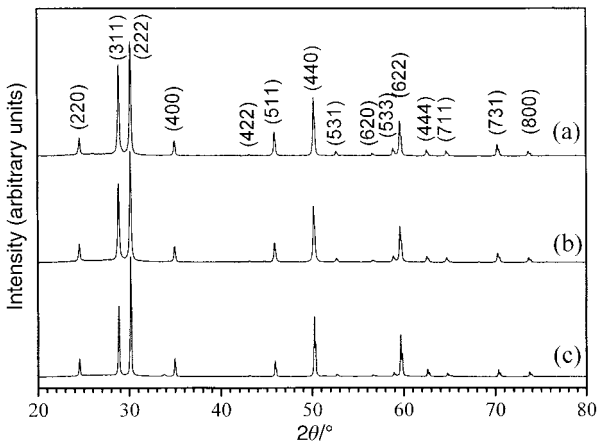

Fig. 2 Powder XRD patterns of Tl–Sb–O phases prepared at 650 °C. (a) Tl/Sb = 1/4, (b) Tl/Sb = 1/3, and (c) Tl/Sb = 1/2.

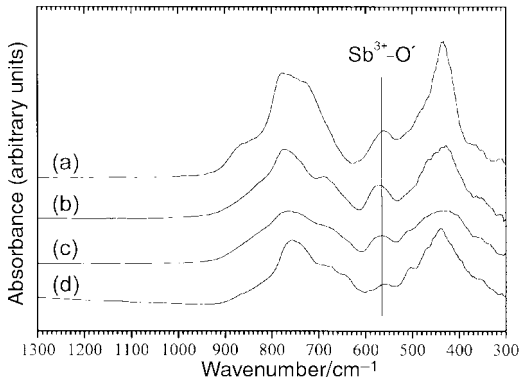

Fig. 3 FT-IR spectra of (a) Sb_6O_{13}, (b) Tl/Sb = 1/4, (c) Tl/Sb = 1/3, (d) Tl/Sb = 1/2. For comparison, the FT-IR spectrum of Sb_6O_{13} is included.

Tl^{3+} cations were transferred into 16d sites, as generally seen in $Tl_2B_2O_6O'$ pyrochlores. Then, the agreement factors were significantly improved to $R_p=11.1\%$, $R_{wp}=11.2\%$, and $R_I=2.76\%$, and the composition was adjusted to $(Tl^{+}{}_{0.55})[Tl^{3+}{}_{0.10}Sb^{3+}{}_{0.57}]Sb_2O_6O'_{0.28}$. In the same way, the Rietveld analyses of the Tl/Sb = 1/3 and 1/2 phases gave the new compositions $(Tl^{+}{}_{0.57})[Tl^{3+}{}_{0.24}Sb^{3+}{}_{0.43}]Sb_2O_6O'_{0.29}$ and $(Tl^{+}{}_{0.58})[Tl^{3+}{}_{0.49}Sb^{3+}{}_{0.18}]Sb_2O_6O'_{0.30}$. In particular for Tl/Sb = 1/2, we tried to refine the compositions $[Tl^{3+}]Sb_2O_6O'_{0.5}$ and $(Tl^{+}{}_{0.5})[Tl^{3+}{}_{0.5}]Sb_2O$, but they were ruled out because of their high agreement factors of $R_{wp}=47\%$ and $R_{wp}=16\%$. The

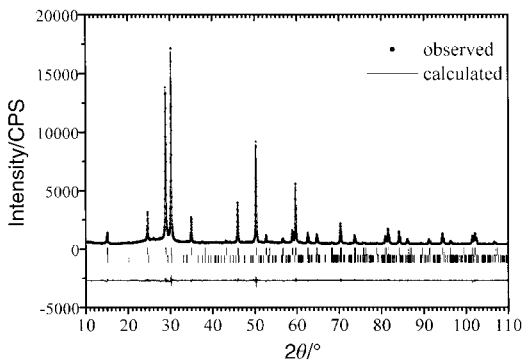

Fig. 4 Observed, calculated, and difference powder XRD profiles of $(Tl^{+}{}_{0.55})[Tl^{3+}{}_{0.10}Sb^{3+}{}_{0.57}]Sb_2O_6O'_{0.28}$ (Tl/Sb = 1/4). The two series of tick marks above the difference plot indicate the Bragg positions for the pyrochlore phase (upper ticks) and Sb_2O_4 (lower ticks, $\sim$1%).

Table 2 Crystallographic data of Tl–Sb–O phases

	Atom	Site	x	y	z	B_{iso}/Å^2
Tl/Sb = 1/4	Tl(1)	16d	0.5	0.5	0.5	1.09(2)
a = 10.3073(1) Å	Sb(1)	96g	0.4992(4)	0.4992(4)	0.5481(4)	1.09(2)
R_p = 11.1%	Sb(2)	16c	0	0	0	1.09(2)
R_{wp} = 11.2%	O(1)	48f	0.3223(3)	1/8	1/8	1.4(1)
R_I = 2.76%	O(2)	8b	3/8	3/8	3/8	1.4(1)
χ^2 = 1.83	Tl(2)	32e	0.3477(1)	0.3477(1)	0.3477(1)	1.09(2)
Tl/Sb = 1/3	Tl(1)	16d	0.5	0.5	0.5	0.79(2)
a = 0.2957(2) Å	Sb(1)	96g	0.4985(6)	0.4985(6)	0.5499(5)	0.79(2)
R_p = 11.3%	Sb(2)	16c	0	0	0	0.79(2)
R_{wp} = 11.5%	O(1)	48f	0.3227(3)	1/8	1/8	1.3(1)
R_I = 3.09%	O(2)	8b	3/8	3/8	3/8	1.3(1)
χ^2 = 1.80	Tl(2)	32e	0.3464(1)	0.3464(1)	0.3464(1)	0.79(2)
Tl/Sb = 1/2	Tl(1)	16d	0.5	0.5	0.5	0.60(2)
a = 10.28204(8) Å	Sb(1)	96g	0.498(1)	0.498(1)	0.552(2)	0.60(2)
R_p = 11.3%	Sb(2)	16c	0	0	0	0.60(2)
R_{wp} = 11.6%	O(1)	48f	0.3243(3)	1/8	1/8	1.1(1)
R_I = 3.34%	O(2)	8b	3/8	3/8	3/8	1.1(1)
χ^2 = 1.97	Tl(2)	32e	0.3454(1)	0.3454(1)	0.3454(1)	0.60(2)

final agreement factors, unit cell parameters, and structural data with their esds in parentheses are listed in Table 2.

Some selected bond distances are listed in Table 3. The bond distances of Sb(1)–O and Sb(2)–O are comparable to those found in single crystal $Tl_{0.51}Sb_{2.71}O_{6.32}$, indicating oxidation states of Sb^{3+}(1) and Sb^{5+}(2). For Tl cations, there are two bond distances (average for phases Tl/Sb = 1/4, 1/3 and 1/2) of Tl(1)–O, 2.479–2.495 Å, and three Tl(2)–O, 3.154–3.182 Å, which are consistent with that (2.449 Å) of Tl^{3+}–O in $Tl_2Ru_2O_7$ and that (3.234 Å) of Tl^{+}–O in $TlNbTeO_6$, confirming the oxidation states of Tl^{3+}(1) and Tl^{+}(2). To gain insight for the oxidation states, bond valence sums (BVS) were calculated using the bond distances obtained. The most commonly adopted empirical expression for the variation of the length d_{ij} of a bond with valence is $v_{ij} = \exp[(R_{ij} - d_{ij})/b]$, where v_{ij} is the bond valence between two atoms i and j, d_{ij} is the cation–oxygen distance and R_{ij} is the bond-valence parameter for the corresponding cation–oxygen bond.[18] The BVS of the Sb^{5+} cation is inversely proportional to those of the Tl^{3+} and Sb^{3+} cations, as listed in Table 4. In $A_2B_2O_6O'$ the oxide ions, O(1), are connected to both A and B cations, that is, the more covalent A–O(1) bond and more ionic B–O(1) bond. Because

Table 3 Selected bond distances of Tl–Sb–O phases

Tl/Sb	1/4	1/3	1/2
Tl(1)–O(1)	6 × 2.583(2)	6 × 2.578(2)	6 × 2.563(2)
Tl(1)–O(2)	2 × 2.2316	2 × 2.2291	2 × 2.2261
Tl(2)–O(1)	3 × 3.256(3)	3 × 3.232(3)	3 × 3.219(2)
	3 × 3.425(3)	3 × 3.433(3)	3 × 3.419(3)
	3 × 2.866(3)	3 × 2.848(3)	3 × 2.825(3)
Sb(1)–O(1)	2 × 2.374(5)	2 × 2.360(6)	2 × 2.34(1)
	1 × 2.963(4)	1 × 2.977(6)	1 × 2.98(1)
	2 × 2.865(4)	2 × 2.872(6)	2 × 2.87(1)
	1 × 2.250(4)	1 × 2.226(6)	1 × 2.20(1)
Sb(1)–O(2)	1 × 2.542(4)	1 × 2.545(5)	1 × 2.56(1)
	1 × 1.997(4)	1 × 1.997(6)	1 × 1.99(1)
Sb(2)–O(1)	6 × 1.969(2)	6 × 1.970(2)	6 × 1.972(2)

Table 4 Bond valence sum of Tl–Sb–O phases

Tl/Sb	1/4	1/3	1/2
Valence (Tl^{+})	0.72	0.75	0.79
Valence (Tl^{3+})	2.33	2.35	2.42
Valence (Sb^{3+})	2.55	2.60	2.69
Valence (Sb^{5+})	5.58	5.56	5.53

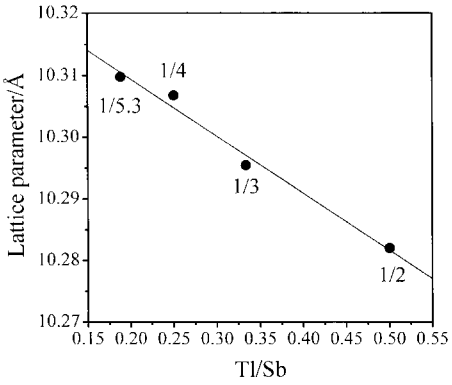

Fig. 5 Plot of unit cell parameter *versus* Tl/Sb ratio.

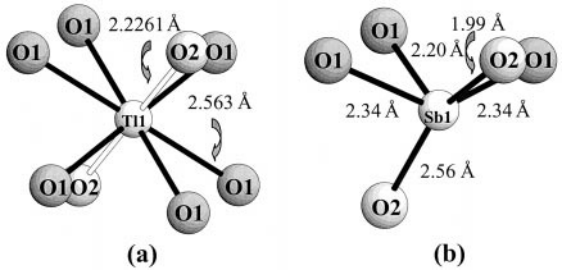

Fig. 6 Coordination environments of (a) Tl^{3+} cation in 16d and (b) Sb^{3+} in 96g sites for the Tl/Sb = 1/2 phase.

the O(1) is also bonded to A′ cations in $A'B_2O_6$, the BVS of the A cations would be also inversely proportional to that of the B cations. We carried out XPS analysis to confirm the oxidation states of Tl^{+}, Tl^{3+}, Sb^{3+}, and Sb^{5+} cations; unfortunately, no clear resolution of the peaks of Tl $4f_{7/2}$ was observed due to the small binding energy difference.[9]

Fig. 5 shows the change of the unit cell parameter as a function of Tl/Sb ratio. Although the ionic radius (0.88 Å) of the Tl^{3+} cation is larger than that (0.76 Å) of the Sb^{3+} cation, the unit cell parameter decreased linearly as the Tl/Sb ratio was increased. Cheihk-Rouhou *et al*. explained that the decrease of unit cell parameter in Sb-doped $Tl_2Mn_2O_7$ was due to the coexistence of Sb^{5+}–Mn^{2+}, indicating not $Tl^{3+}{}_{2-x}Sb^{3+}{}_x$-$Mn^{4+}{}_2O_7$ but $(Tl^{3+}{}_{2-x}Mn^{2+}{}_x)(Mn^{4+}{}_{2-x}Sb^{5+}{}_x)O_7$.[19] However, it is of note here that Sb^{3+} cations are displaced from symmetric 16d to asymmetric 96g sites, resulting in a different coordination environment of Sb^{3+} cations with $4s^2$ lone-pair electrons as shown in Fig. 6. This could be understood as a consequence of the electrostatic repulsion between the lone-pair electrons of Sb^{3+} cations and the bonding pair electrons of Sb–O bonds. According to Shannon, when Bi^{3+} cations are forced into highly symmetric sites, a Bi^{3+}-containing compound has a smaller volume than a La^{3+}-containing one. Meanwhile, when the lone-pair character of Bi^{3+} cations is dominant, the local environment of the Bi^{3+} cations is distorted and both Bi^{3+} and La^{3+} compounds have approximately equal volumes.[20] In this respect, the substitution of Sb^{3+} cations for Tl^{3+} may contribute to the decrease of the unit cell.

Discussion

The refined compositions of Tl–Sb–O pyrochlore phases gave us insight into the structure of pyrochlore $(Tl^{+}{}_{2/3})[Tl^{3+},Sb^{3+}]_{2/3}Sb_2O_6O'_{1/3}$. One can consider it as an intergrown compound of $2/3Tl^{+}Sb_2O_6^{-}$ and $1/3[Tl^{3+},Sb^{3+}]_2Sb_2O_7^{2+}$. In general, the B_2O_6 network is always more stable than the A_2O' in $A_2B_2O_6O'$, and both A and O′ vacancies can exist. In this

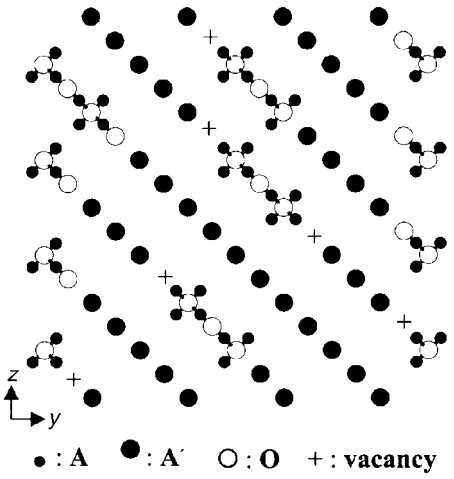

Fig. 7 Schematic 2-dimensional diagram $(Tl^{+}_{2/3-2\delta})[Tl^{3+}_{1-y}Sb^{3+}_{y}]_{2/3}Sb_2O_6O'_{1/3-\delta}$, along the (100) direction, where the vacancies at 16d sites are omitted for clarity.

Table 5 Crystallographic sites for A and A′ cations in several pyrochlore compounds

Compound	8b	32e	16d	96g	Ref.
$TlNbTeO_6$		Tl^+			5
$Tl_2Mn_2O_6O'$			Tl^{3+}		4
$CsBi_2Nb_5O_{16}$	Cs^+, O^{2-}		Bi^{3+}		21
$Ag_{0.63}Sb_{0.50}Sb_2O_6O'_{0.1}$	O^{2-}		Ag^+, Sb^{3+}		9
$Tl_{0.51}Sb_{0.71}Sb_2O_6O'_{0.32}$	O^{2-}	Tl^+		Sb^{3+}	11
$Tl_{0.57}Tl_{0.24}Sb_{0.43}Sb_2O_6O'_{0.29}$	O^{2-}	Tl^+	Tl^{3+}	Sb^{3+}	This work

regard, if $x[Tl^{3+},Sb^{3+}]_2O'$ and Sb_2O_6 firstly build up the pyrochlore structure as interchain and network, the obtained phases are expressed as $[Tl^{3+},Sb^{3+}]Sb_2O_6O'_{0.5}$ ($x=1/2$), $[Tl^{3+},Sb^{3+}]_{2/3}Sb_2O_6O'_{1/3}$ ($x=1/3$), and so on. The composition $[Tl^{3+},Sb^{3+}]_{2/3}Sb_2O_6O'_{1/3}$ induces a net negative charge of 2/3, which is neutralized by introducing metal cations such as Tl^{3+}. Therefore, one can describe Tl–Sb–O pyrochlore phases by the formula $(Tl^{+}_{2/3})[Tl^{3+},Sb^{3+}]_{2/3}Sb_2O_6O'_{1/3}$.

One point to note is that the occupation factor of the (Tl^+,O') in $(Tl^{+}_{2/3})[Tl^{3+},Sb^{3+}]_{2/3}Sb_2O_6O'_{1/3}$ is smaller than unity, as shown in Tl/Sb = 1/5.3–1/2. For the purpose of discussion one can consider that both Tl^+ and O' are in '8b' sites, and both Tl^{3+} and Sb^{3+} are in '16d' sites. Then, these compositions can be viewed as the random distribution of $2/3A'B_2O_6$ and $1/3A_2B_2O_6O'$ in a domain as shown in Fig. 7. Because adjacent '8b' and '16d' sites cannot be simultaneously occupied by cations having a radius exceeding around 1.1 Å, the most favorable coordination would be Tl^+ in '8b' sites, vacant '16d' sites and $[Tl^{3+},Sb^{3+}]$ in '16d' sites, O' in '8b', respectively. Therefore, it is natural that the vacancies at '8b' sites, marked by '+' in Fig. 7, exist in the compound, in addition to vacant '16d' sites. The Tl–Sb–O phases synthesized can be described as the formula $(Tl^{+}_{2/3-2\delta})[Tl^{3+}_{1-y}Sb^{3+}_{y}]_{2/3}Sb_2O_6O'_{1/3-\delta}$, where $\delta \sim 0.05$. In this regard, $RbBi_2Ta_5O_{16}$ can be considered as $(Rb_{0.4})[Bi_{0.8}]Ta_2O_6O'_{0.4}$ ($x=0.4$, $\delta=0$).[21] Finally, the measured densities of 6.50, 6.79, and 7.02 g cm^{-3} for Tl/Sb = 1/4, 1/3, and 1/2 are in good agreement with theoretical densities of 6.626, 6.841, and 7.147 g cm^{-3}, confirming the suggested formula.

In conclusion, we have prepared and characterised the new defect pyrochlore phase $(Tl^{+}_{2/3-2\delta})[Tl^{3+}_{1-y}Sb^{3+}_{y}]_{2/3}Sb_2O_6O'_{1/3-\delta}$, which is a quite unique pyrochlore phase in that Tl and Sb cations, involving the displacement of Sb^{3+} cations, are randomly positioned in 16d, 32e and 96g sites. In fact, one should keep in mind that the formula obtained here may be considered as a structural model rather than an accurate structure, owing to the fact that the pyrochlore structure enables many substitutions leading to new compositions. These Tl–Sb–O phases would provide a new concept in defect pyrochlores with various compositions. Although a large number of pyrochlore phases have been reported, most of them have the normal compositions of $A'B_2O_6$ or $A_2B_2O_6O'$, as listed in Table 5. As far as we know, $(Tl^{+}_{2/3-2\delta})[Tl^{3+}_{1-y}Sb^{3+}_{y}]_{2/3}Sb_2O_6O'_{1/3-\delta}$ is the first example in which three A/A′ cations are simultaneously shown in a pyrochlore structure.

Acknowledgements

The authors gratefully acknowledge the direct support of this work by the Ministry of Education.

References

1 J. B. Goodenough, H. Y-P. Hong and J. A. Kafalas, *Mater. Res. Bull.*, 1976, **11**, 203.
2 P. J. Wilde and C. R. A. Catlow, *Solid State Ionics*, 1998, **112**, 173.
3 Y. Shimakawa, Y. Kubo and T. Manako, *Nature*, 1996, **379**, 53.
4 M. A. Subramanian, B. H. Tody, A. P. Ramirez, W. J. Harshall, A. W. Sleight and G. H. Kwei, *Science*, 1996, **273**, 81.
5 B. Darriet, M. Rat, J. Galy and P. Hagenmuller, *Mater. Res. Bull.*, 1971, **6**, 1305.
6 M. A. Subramanian, G. Aravamudan and G. V. Subba Rao, *Prog. Solid State Chem.*, 1983, **15**, 55.
7 J. L. Fourquet, H. Duroy and Ph. Lacorre, *J. Solid State Chem.*, 1995, **114**, 575.
8 H. Mizoguchi, H. Kawazoe, T. Ueda, S. Hayashi, H. Hosono and N. Ueda, *Bull. Chem. Soc. Jpn.*, 1996, **69**, 111.
9 A. J. G. Zarbin, O. L. Alves, J. M. Amarilla, R. M. Rojas and J. M. Rojo, *Chem. Mater.*, 1999, **11**, 1652.
10 G. M. Kales and S. Srikanth, *J. Am. Ceram. Soc.*, 1999, **82**, 2161.
11 Y. Piffard and M. Tournoux, *Acta Crystallogr., Sect. B*, 1979, **35**, 1450.
12 A. Haddad, T. Jouini, A. Verbaere, Y. Piffard and J. C. Jumas, *J. Solid State Chem.*, 1994, **109**, 181.
13 Y. Piffard, M. Dion and M. Tournoux, *Acta Crystallogr., Sect. B*, 1978, **34**, 366.
14 T. S. Ercit, P. Cerny and F. C. Hawthorne, *Mineral. Petrol.*, 1993, **48**, 235.
15 R. C. Rouse, P. J. Dunn, D. R. Peacor and L. Wang, *J. Solid State Chem.*, 1998, **141**, 562.
16 J. Rodriguez-Carvajal, *Program Fullprof*, version 3.2, January 1997, LLB JRC.
17 Y. Xuan, R. Liu and Y. Q. Jia, *Mater. Chem. Phys.*, 1998, **53**, 156.
18 N. E. Brese and M. O'Keeffe, *Acta Crystallogr., Sect. B*, 1991, **47**, 192.
19 W. Cheihk-Rouhou, P. Strobel, C. Chaillout, S. M. Loureiro, R. Senis, B. M. Martinez, X. Obradors and J. Pierre, *J. Mater. Chem.*, 1999, **9**, 743.
20 R. D. Shannon, *Acta Crystallogr., Sect. A*, 1976, **32**, 751.
21 M. K. Ehlert, J. E. Greedan and M. A. Subramanian, *J. Solid State Chem.*, 1988, **75**, 188.